Available online at www.sciencedirect.com
SCIENCE DIRECT®
Journal of Power Sources 124 (2003) 204–212
JOURNAL OF POWER SOURCES
www.elsevier.com/locate/jpowsour

Iron–tin oxides with $CaFe_2O_4$ structure as anodes for Li-ion batteries

N. Sharma, K.M. Shaju, G.V. Subba Rao, B.V.R. Chowdari*

Department of Physics, National University of Singapore, Singapore 119260, Singapore

Received 20 April 2003; accepted 4 June 2003

Abstract

To investigate the effect of matrix, counter ions and cycling conditions on the properties of mixed iron oxides, $CaFe_2O_4$, $Li_{0.5}Ca_{0.5}(Fe_{1.5}Sn_{0.5})O_4$ and $NaFeSnO_4$ have been synthesized and their electrochemical performance studied. $CaFe_2O_4$ shows a reversible capacity of ~200 mAh g^{-1} at 60 mA g^{-1} and 12–50 cycles in the range 0.005–3.0 V, but shows slight capacity fading when the upper voltage is reduced to 2.5 V. $Li_{0.5}Ca_{0.5}(Fe_{1.5}Sn_{0.5})O_4$ gives a reversible capacity of ~450 mAh g^{-1} in the voltage range 0.005–3.0 V at a current density of 60 mA g^{-1} over 5–30 cycles and shows slight capacity-fading up to 50 cycles. $NaFeSnO_4$ displays drastic capacity-fading on cycling to 3.0 V, but has very good cycling performance (310–340 mAh g^{-1} for to 4–110 cycles) on cycling between 0.005 and 1.0 V at 60 mA g^{-1}. The mechanism of operation of the electrodes, as well as the beneficial effects of the presence of Ca ions and cycling up to a 3.0 V cut-off in the Ca-ferrites, are discussed.

Keywords: Li-ion battery; Anode material; Ca-ferrite; $NaFeSnO_4$; Cycle performance

1. Introduction

Studies of anode materials for Li-ion batteries have focused on carbonaceous materials [1], tin (Sn) oxides and amorphous tin composite oxides (ATCOs) [2–6], Li-alloys and intermetallics [7], and recently, transition metal oxides [8–13]. The higher capacity observed for the latter materials (i.e. 400–900 mAh g^{-1}) compared with graphite (theoretical capacity: 372 mAh g^{-1}) together with beneficial safety aspects make these materials an alternative choice as anodes in lithium-ion batteries. Accordingly, extensive studies were carried out to explore the materials and optimize their performance.

The reversible formation of Li–Sn alloy contributes to the capacity of Sn-oxides and ATCOs. An ATCO with boron and phosphorous was reported to exhibit reversible capacity values as high as 600 mAh g^{-1} [2], but a large irreversible capacity loss during the first-discharge and its limited cycle-life due to aggregation of Sn-metal particles over repeated charge–discharge cycling has limited its use in practical cells. Several strategies have been adopted to overcome the problem of capacity-fading in ATCO and other Sn-containing compounds, for example by using 'spectator' atoms in the matrix that can help in absorbing the volume changes that take place during cycling and retard the Sn-aggregation process [3–6], by dispersing the electroactive Sn-oxide in the form of nano-particles, and by choosing the appropriate operating potential window [3–5].

Recently, transition metal oxide MO (M: Co, Ni, Cu and Fe) have been studied as possible anodes [8–13]. A reaction mechanism for these oxides that involves the formation and decomposition of Li_2O accompanied by the oxidation and reduction of metal nano-particles has been proposed [8–10,12,13]. As for Sn-compounds, these transition metal oxides suffer from irreversible capacity loss on the first cycle. The possible cause is the irreversible formation of a solid electrolyte interphase (SEI) as a consequence of electrolyte decomposition that involves lithium. The oxide CoO was found to show the best performance with reversible capacities as high as 700 mAh g^{-1} and good capacity retention for more than 50 cycles [8,9]. On other hand, studies by Wang et al. [12,13] and Larcher et al. [14] showed that CoO and Co_3O_4 display significant capacity-fading on cycling, especially in the case of Co_3O_4. Iron oxide has also given promising initial capacity values (300–600 mAh g^{-1}), but exhibits significant capacity-fading on continued cycling [8]. Iron oxides are attractive materials for lithium-ion batteries due to their abundance, low cost and environmentally benign discharge products. Mixed oxides of iron, $FeBO_3$ [15] and Fe_3BO_6 [15,16], $CaFe_2O_4$ and Li–Ca–Fe–SnO_4 [11,17] have been studied in terms of their anodic properties. Our recent studies on $CaSnO_3$ have shown that Ca acts as a beneficial 'spectator' atom in giving and sustaining high

* Corresponding author. Tel.: +65-6874-2956; fax: +65-6777-6126.
E-mail address: phychowd@nus.edu.sg (B.V.R. Chowdari).

0378-7753/$ – see front matter © 2003 Elsevier B.V. All rights reserved.
doi:10.1016/S0378-7753(03)00670-0

capacity (380 mAh g^{-1}) over repeated charge–discharge cycles [5]. This work reports investigations on $CaFe_2O_4$ and its Sn doped compounds, $Li_{0.5}Ca_{0.5}(Fe_{1.5}Sn_{0.5})O_4$ and $NaFeSnO_4$, for use as anode materials in lithium-ion batteries, and on the effect of Ca as a 'spectactor' atom in the matrix.

2. Experimental

The compounds $CaFe_2O_4$, $Li_{0.5}Ca_{0.5}(Fe_{1.5}Sn_{0.5})O_4$ and $NaFeSnO_4$ were synthesized by means of a high temperature solid-state reaction. The starting materials used for the synthesis were: Li_2CO_3 (Fluka), Na_2CO_3, $CaCO_3$ (Merck), SnO_2 (Merck) and Fe_2O_3 (Fisher). For the preparation of $CaFe_2O_4$ and $Li_{0.5}Ca_{0.5}(Fe_{1.5}Sn_{0.5})O_4$, stoichiometric amounts of the starting materials were mixed, ground and heated at 1180 °C in air for 24 h, followed by quenching to room temperature. The product was reground, re-heated as above and quenched [17,18]. For $NaFeSnO_4$ preparation, a thoroughly ground stoichiometric mixture of the reactants was heated at 850 °C for 24 h, followed by slow cooling (3 °C per min) to room temperature. The reground product was pelletized and subjected to the same heat treatment. The final product was ground to a fine powder.

Structural characterization of the compounds was done by powder X-ray diffraction (XRD) using a Siemens D5005/difractometer equipped with Cu Kα radiation. The morphology of the powders was examined by scanning electron microscopy (SEM, JEOL JSM-6700F, Field Emission Electron Microscope). Composite electrodes of the active materials for electrochemical studies were made with the mixed oxide, Super P carbon and binder (Kynar 2801) in the weight ratio 65:15:20. A thick slurry of the respective mixtures was made using *N*-methyl pyrrolidone (NMP) as the solvent. The slurry was coated on a copper foil by the doctor-blade technique [5]. The thick film (20–30 μm) electrodes were dried at 80 °C in an air oven for 24 h, pressed between twin rollers, cut into circular discs (16 mm diameter), and then vacuum dried at 70 °C for 12 h. These were transferred to an agron-filled glove-box which maintains <1 ppm of H_2O and O_2 (MBraun, Germany). Coin cells (size 2016) were fabricated in the glove box with lithium metal (Kyokuto metal Co., Japan) as the counter electrode, Celgard 2502 membrane as the separator, and 1 M $LiPF_6$ in ethylene carbonate (EC) + diethyl carbonate (DEC) (1:1 by volume, Merck Selectipur LP40) as the electrolyte. Cyclic voltammetry (CV) and galvanostatic charge–discharge cycling of the cells were performed with a MacPile II (Biologic, France) and Bitrode multiple battery tester (model SCN, Bitrode, USA).

3. Results and discussion

The XRD patterns of the compounds, $CaFe_2O_4$, $Li_{0.5}Ca_{0.5}(Fe_{1.5}Sn_{0.5})O_4$ and $NaFeSnO_4$ are shown in Fig. 1a–c. The lattice parameters were determined by least squares fitting of the 2θ and *hkl* values. The pattern of $CaFe_2O_4$ has been indexed according to the JCPDS database

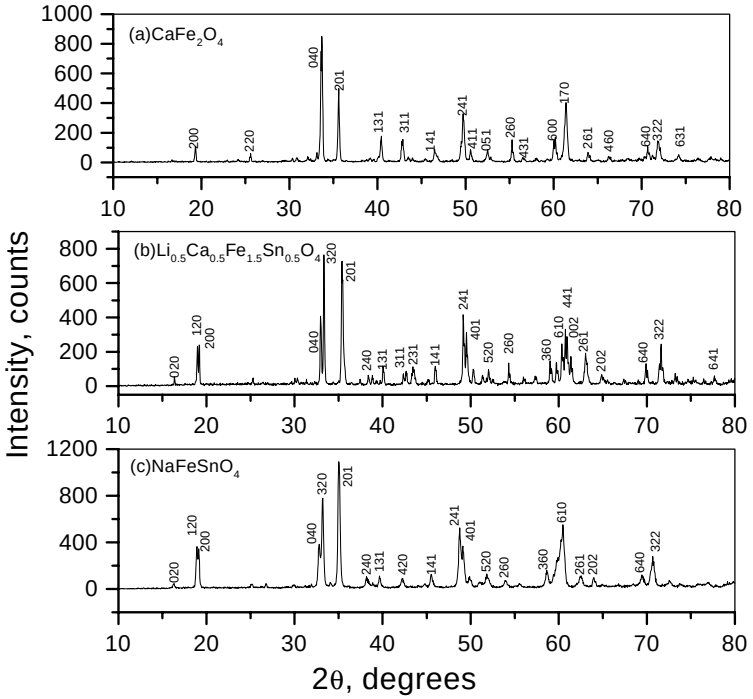

Fig. 1. Powder X-ray diffraction (XRD) patterns for compounds, $CaFe_2O_4$, $Li_{0.5}Ca_{0.5}(Fe_{1.5}Sn_{0.5})O_4$ and $NaFeSnO_4$. Miller indices (*hkl*) are shown.

(file no. 32-0168) and the orthorhombic lattice parameters are: $a = 9.219\ (\pm 0.007)$ Å, $b = 10.70\ (\pm 0.01)$ Å, $c = 3.015\ (\pm 0.003)$ Å. These are in good agreement with the literature reports [17,18]. The $CaFe_2O_4$ framework is built from the vertex sharing of double rutile-type units of FeO_6 octahedral that form pesudo-triangular tunnels which are occupied by Ca^{2+} ions [17,18]. This structure is known to have compositional flexibility, and *iso*-structural solid solutions are possible by replacing Fe by Sn with an accompanying substitution of Ca by Li with the formula, $Li_yCa_{1-(x+y)/2}(Sn_xFe_{2-x})O_4$, and $0 < y < x$ and $0 < x < 0.6$. Such solid solutions have been found to have better electrical conductivity when $x = y$ [18]. The XRD pattern of the solid solution, $Li_{0.5}Ca_{0.5}(Fe_{1.5}Sn_{0.5})O_4$ ($x = y = 0.5$) has been indexed. The lattice parameters are: $a = 9.287\ (\pm 0.002)$ Å, $b = 10.88\ (\pm 0.01)$ Å, $c = 3.025\ (\pm 0.005)$ Å and are in agreement with reported values [17,18]. $NaFeSnO_4$ is *iso*-structural with $CaFe_2O_4$ [19] and its orthorhombic lattice parameters ($a = 9.303\ (\pm 0.006)$ Å, $b = 10.95\ (\pm 0.01)$ Å, $c = 3.067\ (\pm 0.002)$ Å) match well with the reported data in the JCPDS file (no. 73-0425), except that *b* and *c* are now interchanged. No impurity phases are noticed in the XRD patterns of the above three compounds. Electron micrographs of the compounds are shown in Fig. 2. It can be seen that $CaFe_2O_4$ and $Li_{0.5}Ca_{0.5}(Fe_{1.5}Sn_{0.5})O_4$ have large (5–8 μm size), plate-like, non-uniform crystallites, whereas $NaFeSnO_4$ consists of very fine and uniform crystallites with sizes, 200–400 nm. The lower synthesis-temperature of $NaFeSnO_4$ assists in obtaining fine particles.

The electrochemical performance of the compounds was evaluated in half-cell configuration with a Li-metal anode. For galvanostatic as well as for potentiostatic cycling, the first scan always commenced in a negative direction from the open-circuit voltage of the cell.

For galvanostatic charge–discharge cycling, the cells were cycled at a current density of 10 mA g^{-1} for the first 2 cycles and thereafter at 60 mA g^{-1} in the voltage range 0.005–2.5 or 0.005–3.0 V. The voltage versus capacity profiles for the first-discharge and first-charge cycle (at 10 mA g^{-1}) for the compounds, $CaFe_2O_4$ and $Li_{0.5}Ca_{0.5}(Fe_{1.5}Sn_{0.5})O_4$ are presented in Fig. 3a. The corresponding voltage profiles for different charge–discharge cycles (0.005–2.5 V; 5–50 cycles, only select cycles are shown for clarity) at a current density of 60 mA g^{-1} are given in Fig. 3b and c, respectively. The voltage versus capacity profile for the first-discharge and first-charge cycle (at 10 mA g^{-1}) for $NaFeSnO_4$ in the voltage range 0.005–1.0 and 0.005–3.0 V is presented in Fig. 4a. The profiles at 60 mA g^{-1} (2nd cycle at 10 mA g^{-1}) for different charge–discharge cycles and voltage ranges are given in Fig. 4b and c. The first-discharge profiles (Figs. 3a and 4a) for all the compounds exhibit a plateau in the range 1.0–0.5 V until capacity of 600–800 mA g^{-1} is reached. Thereafter, the voltage decreases gradually to 0.005 V.

The first discharge reaction in the above metal oxides when acting as cathodes versus Li is irreversible destruction of the crystal structure that leads to the formation of metal nano-particles embedded in an amorphous matrix of CaO and Li_2O [6,8–12,17,20–22], i.e.

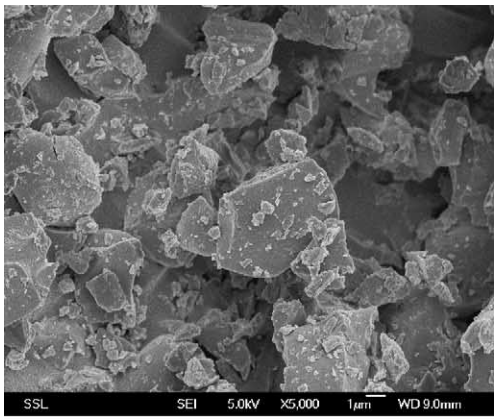

(a)

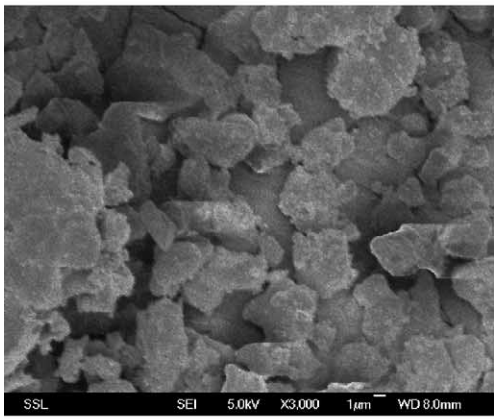

(b)

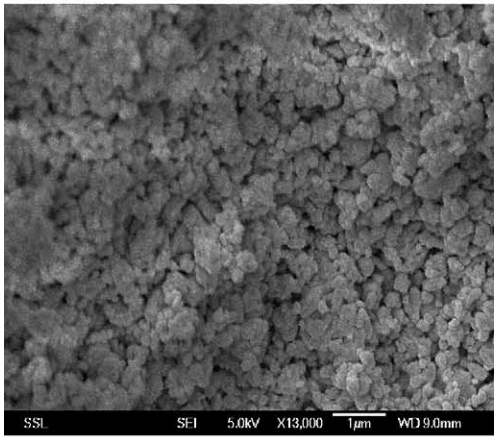

(c)

Fig. 2. Scanning electron micrographs of (a) $CaFe_2O_4$; (b) $Li_{0.5}Ca_{0.5}(Fe_{1.5}Sn_{0.5})O_4$; and (c) $NaFeSnO_4$.

$$CaFe_2{}^{3+}O_4 + 6Li^+ + 6e^- \rightarrow CaO + 2Fe + 3Li_2O \quad (1)$$

$$Li_{0.5}Ca_{0.5}(Fe_{1.5}Sn_{0.5})O_4 + 6.5Li^+ + 6.5e^- \rightarrow 0.5CaO + 1.5Fe + 0.5Sn + 3.5Li_2O \quad (2)$$

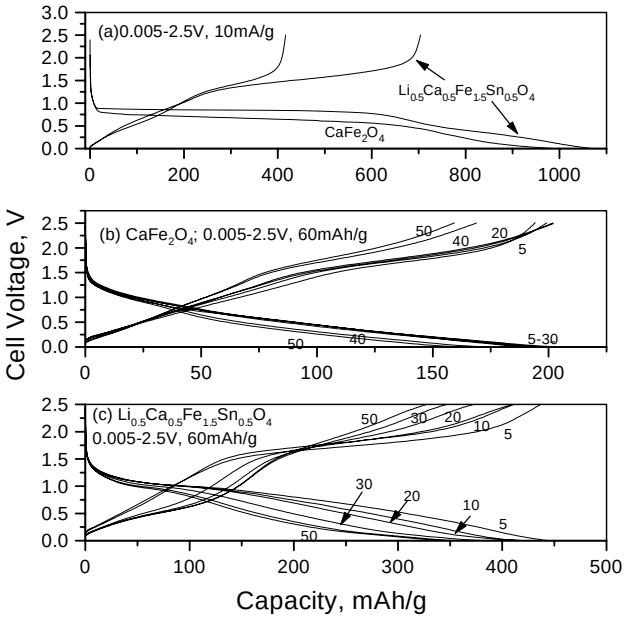

Fig. 3. Voltage vs. capacity profiles for $CaFe_2O_4$ and $Li_{0.5}Ca_{0.5}(Fe_{1.5}Sn_{0.5})O_4$. (a) First discharge (OCV to 0.005 V) and charge (0.005–2.5 V) curves at 10 mA g^{-1}. Profiles during 5–50 cycles at 60 mA g^{-1} and in voltage range 0.005–2.5 V: (b) $CaFe_2O_4$; (c) $Li_{0.5}Ca_{0.5}(Fe_{1.5}Sn_{0.5})O_4$. Cycle numbers are indicated.

$$NaFe^{3+}Sn^{4+}O_4 + 7Li^+ + 7e^- \rightarrow 0.5Na_2O + Fe + Sn + 3.5Li_2O \quad (3)$$

In $Li_{0.5}Ca_{0.5}(Fe_{1.5}Sn_{0.5})O_4$ and $NaFeSnO_4$, reactions (2) and (3) are also accompanied by alloy formation of Sn with Li metal, i.e.

$$Sn + 4.4Li^+ + 4.4e^- \leftrightarrow Li_{4.4}Sn \quad (4)$$

On the subsequent charging, the reverse of reaction (4) occurs in the low voltage region (<1.5 V), but in the high voltage range the metal (Fe) particles are converted to oxide together with the decomposition of Li_2O which can be written as:

$$Fe + Li_2O \leftrightarrow FeO + 2Li^+ + 2e^- \quad (5)$$

This reversible displacement reaction, viz., the formation and decomposition of Li_2O accompanied by the reduction and oxidation of metal nano-particles together with the alloying–de-alloying of Sn with Li gives rise to reversible capacity in subsequent cycles. Thus, cycling proceeds in a reversible three-phase region between metal oxide, the metals (Fe, Sn and alloy $Li_{4.4}Sn$) and Li_2O. Calcium metal does not form during the first discharge due to the high Ca–O

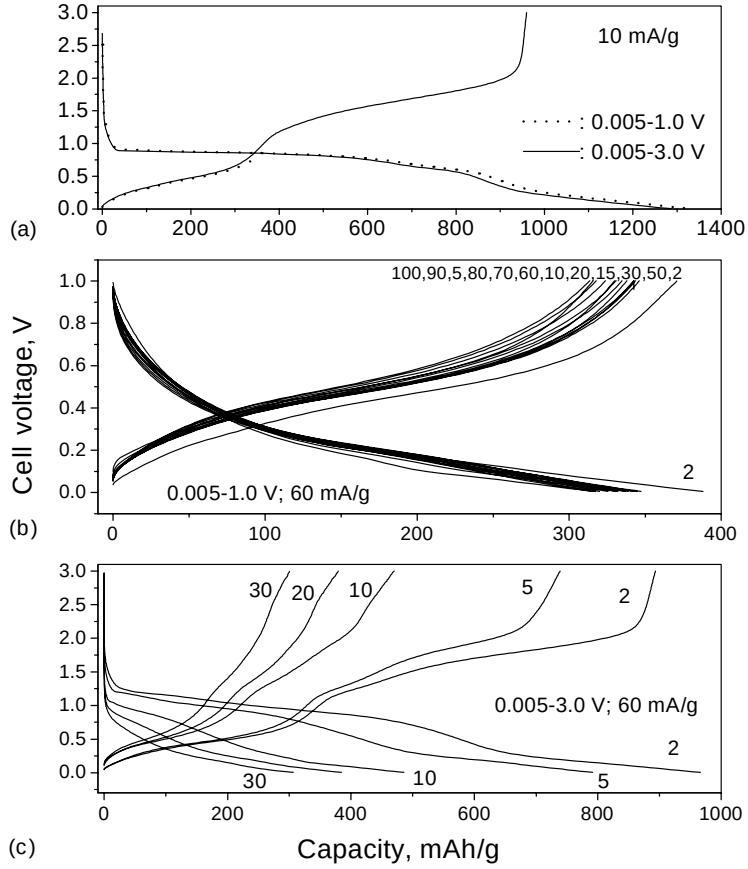

Fig. 4. Voltage vs. capacity profiles for $NaFeSnO_4$. (a) First discharge (OCV to 0.005 V) and charge (0.005–1.0 V and 0.005–3.0 V) curves at 10 mA g^{-1}; (b) profiles during 2–100 cycles in voltage window 0.005–1.0 V at 60 mA g^{-1} (2nd cycle at 10 mA g^{-1}); (c) profiles during 2–30 cycles in voltage window, 0.005–3.0 V at 60 mA g^{-1} (2nd cycle at 10 mA g^{-1}). Only selected cycles are shown. Cycle numbers are indicated.

bond strength [5,20]. Li_2O is known to be electrochemically inactive, but in the case of nano-sized metal particles, chemical and physical phenomena can be affected and the electrochemically-driven size confinement of the metal particles is believed to enhance their electrochemical activity towards the formation/decomposition of Li_2O [8–10,12].

Similarities in the voltage profiles of $CaFe_2O_4$, $Li_{0.5}C_{0.5}(Fe_{1.5}Sn_{0.5})O_4$ and $NaFeSnO_4$ during the first-discharge suggest that the processes of structural destruction (Eqs. (1)–(3)) and alloy formation (Eq. (4)) are not clearly distinguishable. The plateau position corresponding to the first-discharge is almost the same for $Li_{0.5}Ca_{0.5}(Fe_{1.5}Sn_{0.5})O_4$ and $NaFeSnO_4$ (~0.85 V). This is slightly higher than the plateau voltage for $CaFe_2O_4$ (0.7 V), and possibly reflects the effect of Sn substitution and the counter ions (Ca, Na) and its relative ratio present in the compounds. Similar observations have been reported for 3d metal oxides [8–10,12,15,17] and Sn-based compounds [6,20,21], for which the plateau position is found to be sensitive to the chemical composition of the matrix and the crystal structure of the starting oxide, even though the same electrochemical process takes place.

From the first-charge profiles (Fig. 3a), it can be seen that the contribution to capacity increases in $Li_{0.5}Ca_{0.5}(Fe_{1.5}Sn_{0.5})O_4$ (66% of the first-discharge capacity) compared with $CaFe_2O_4$ (43%), as can be expected due to the presence of Sn. The first-charge contribution of $NaFeSnO_4$ is 75% of the first-discharge capacity up to 3.0 V, whereas it is only 30% up to a 1.0 V upper cut-off voltage. The latter behaviour is due to the alloying de-alloying of Sn (Eq. (4)). It is noted that there exists a qualitative difference in the voltage profiles of $Li_{0.5}Ca_{0.5}(Fe_{1.5}Sn_{0.5})O_4$ and $NaFeSnO_4$ during subsequent charge–discharge cycles in the voltage range 0.005–2.5 (or 3.0) V at 60 mA g^{-1}. The plateau corresponding to the reversible reactions (4) and (5) are clearly distinguishable for $NaFeSnO_4$ from the initial cycles (2–10 Fig. 4c), but for $Li_{0.5}Ca_{0.5}(Fe_{1.5}Sn_{0.5})O_4$, the plateaus become clear only after the 20th cycle (Fig. 3c).

The observed first discharge–charge capacity values, the corresponding number of Li atoms (ions + electrons) involved and the expected Li-atoms (calculated as per Eqs. (1)–(4)) are given in Table 1. For all the compounds, observed values corresponding to the first-discharge capacity are higher than the calculated values. For $CaFe_2O_4$, the difference is as much as 2.0 Li per formula unit, whereas for $Li_{0.5}Ca_{0.5}(Fe_{1.5}Sn_{0.5})O_4$ it is only 0.7 Li. This may be explained partly on the basis of reversible formation of polymeric gel layer around the metal nano-particles as observed with 3d metal oxides [9], and also partly to the irreversible formation of a solid electrolyte interphase [5]. Similar high values of the number of Li atoms consumed during the first-discharge have also been reported by Duncan and Nazar [17] in preliminary studies on $CaFe_2O_4$ and $Li_{0.3}Ca_{0.7}(Fe_{1.7}Sn_{0.3})O_4$. The observed capacity values (and the corresponding number of Li atoms) during the first-charge cycle are lower than the calculated values for $CaFe_2O_4$ (Table 1). This may be attributed to the insulating nature of the compound which gives rise to poor charge transfer and, therefore, less than full utilization of the active material. The observed first-charge capacities for the Sn-substituted ferrites $Li_{0.5}Ca_{0.5}(Fe_{1.5}Sn_{0.5})O_4$ and $NaFeSnO_4$ are higher than the calculated values if it is assumed that de-alloying of $Li_{4.4}Sn$ and FeO formation (reactions of Eqs. (4) and (5)) are the only contributing factors. It is possible, however, that oxidation of Sn-metal particles with the simultaneous decomposition of Li_2O matrix can occur on charging to higher voltages (>1.5 V versus Li), i.e.

$$Li_2O + Sn \leftrightarrow 2Li^+ + 2e^- + SnO \quad (6a)$$

$$2Li_2O + Sn \leftrightarrow 4Li^+ + 4e^- + SnO_2 \quad (6b)$$

If the contribution of Eq. (6a) is also included, then the observed and the calculated first-charge capacities match very well for $Li_{0.5}Ca_{0.5}(Fe_{1.5}Sn_{0.5})O_4$ (Table 1). In the case of $NaFeSnO_4$, however, it may also be necessary to include partial contribution to the capacity from Eq. (6b),

Table 1
Observed and calculated discharge–charge capacities and corresponding number of Li atoms per formula unit for stated compounds

Compound	Voltage range of cycling (V vs. Li)	Molecular weight (g)	First discharge capacity (mAh g^{-1}) at 10 mA g^{-1} (no. of Li^+)		First-charge capacity (mAh g^{-1}) at 10 mA g^{-1} (no. of Li^+)		Charge capacity (mAh g^{-1}) at 4th/50th cycle (at 60 mA g^{-1})
			Observed	Calculated	Observed	Calculated[a]	
$CaFe_2O_4$	0.005–2.5	215.8	988 (8.0)	745 (6.0)	419 (3.4)	497 (4.0)	193/160
	0.005–3.0	–	–	–	–	–	200 (13th)/195 (50th)
$Li_{0.5}Ca_{0.5}(Fe_{1.5}Sn_{0.5})O_4$	0.005–3.0	231.2	1097 (9.4)	1009 (8.7)	728 (6.3)	603 (5.2) 719 (6.2)[b]	467/405
	0.005–2.5	–	–	–	–	–	444/342
$NaFeSnO_4$	0.005–3.0	261.6	1286 (12.5)	1168 (11.4)	960 (9.4)	656 (6.4) 861 (8.4)[b]	490 (7th)/275 (35th)
	0.005–1.0	–	–	–	382 (3.7	451 (4.4)	310 (4th)/342 (50th)/313 (110th)

[a] Calculated as per Eqs. (4) and (5).
[b] Includes contributions from Eqs. (4)–(6a).

in addition to Eq. (6a), to explain the discrepancy between the observed and calculated first-charge capacities (Table 1). Such a reversible oxidation of Sn on charging to high voltages has been observed in SnO_2 [4] and $CaSnO_3$ [22]. The fact that higher capacity is observed only in the Sn-substituted $CaFe_2O_4$-type compounds consolidates the above arguments.

The charge–discharge capacity as a function of cycle number (3–50 cycles) for the compounds $CaFe_2O_4$ and $Li_{0.5}Ca_{0.5}(Fe_{1.5}Sn_{0.5})O_4$ at 60 mA g^{-1} between 0.005 and 2.5 V (the first 2 cycles were performed at 10 mA g^{-1}) are shown in Fig. 5(a). The charge and discharge capacity values overlap in all cases, which indicates excellent coulombic efficiency at this fairly high current rate. It is clear from the cycling performance that $Li_{0.5}Ca_{0.5}(Fe_{1.5}Sn_{0.5})O_4$ is superior to $CaFe_2O_4$ in terms of reversible capacity. The higher capacity values for the former material are due to the participation of Sn in the alloying–de-alloying process (Eq. (4)) in addition to the reversible Fe–FeO couple as shown in Eq. (5). Moreover, the presence of two different active host metals (Fe and Sn) and two separate reaction mechanisms (displacive and alloying) probably maintains the electronic conductivity of the electrode. A gradual capacity-fading between 15 and 50 cycles is seen for both

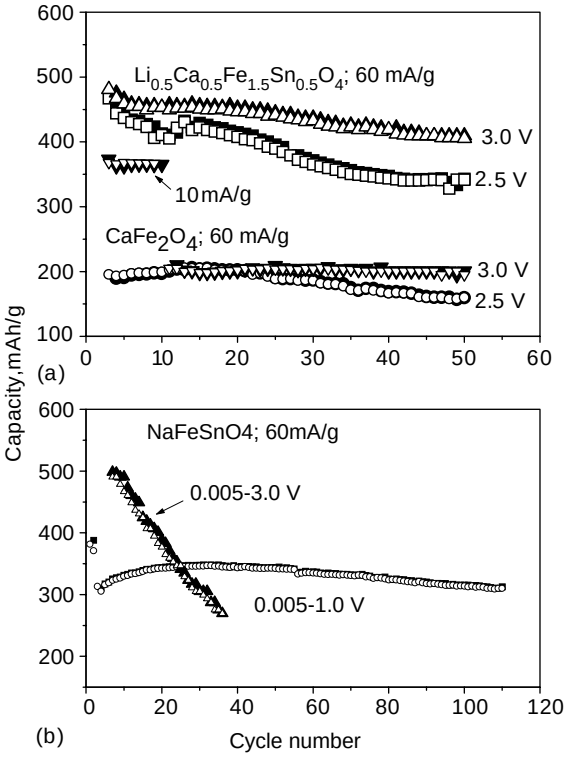

Fig. 5. Charge–discharge capacities as function of cycle number for compounds (first 2 cycles at 10 mA g^{-1}). (a) $CaFe_2O_4$ and $Li_{0.5}Ca_{0.5}(Fe_{1.5}Sn_{0.5})O_4$ in voltage windows 0.005–2.5 and 0.005–3.0 V. Current densities and upper cut-off voltage are shown; (b) $NaFeSnO_4$ at 60 mA g^{-1} between 0.005 and 1.0 V (2–110 cycles; first 2 cycles at 10 mA g^{-1} not shown) and in the range 0.005–3.0 V (6–35 cycles; first 5 cycles at 10 mA g^{-1} not shown). Filled and open symbols are for discharge and charge cycle, respectively.

$Li_{0.5}Ca_{0.5}(Fe_{1.5}Sn_{0.5})O_4$ and $CaFe_2O_4$ when cycled in the range of 0.005–2.5 V. For $Li_{0.5}Ca_{0.5}(Fe_{1.5}Sn_{0.5})O_4$, this may be attributed partially to the sensitivity of Sn-containing compounds towards the operational voltage window for stable performance, as has been observed for SnO_2 and other Sn-based compounds [3–5,21]. On cycling the cells in the voltage range 0.005–3.0 V $Li_{0.5}Ca_{0.5}(Fe_{1.5}Sn_{0.5})O_4$ still shows some capacity-fading, $CaFe_2O_4$ displays excellent capacity-retention up to 50 cycles (Fig. 5a). In their preliminary studies, the group of Nazar [17] has reported a first-charge capacity of 646 mAh g^{-1} for $Li_{0.5}Ca_{0.5}(Fe_{1.5}Sn_{0.5})O_4$ which falls to ~500 mAh g^{-1} at the end of the 25th cycle (at 50 mA g^{-1}; 0.005–3.0 V). For the same compound, this study shows a first-charge capacity of 728 mAh g^{-1} (at 10 mA g^{-1}; 0.005–3.0 V). On increasing the current density to 60 mA g^{-1}, the capacity is 467 mAh g^{-1} on the fourth cycle and remains at 405 mAh g^{-1} at the end of the 50th cycle (Fig. 5a).

The charge–discharge capacity as a function of cycle number for the compound $NaFeSnO_4$ at 60 mA g^{-1} between 0.005 and 1.0 V (2–110 cycles; the first 2 cycles at 10 mA g^{-1}) and between 0.005 and 3.0 V (6–35 cycles; first 5 cycles at 10 mA g^{-1}) is shown in Fig. 5b. On cycling to 3.0 V (upper cut-off voltage), the cell shows a first-charge capacity of 960 mAh g^{-1} which falls to 740 mAh g^{-1} on the fifth cycle (not shown in Fig. 5b). For the subsequent cycles at a current density of 60 mA g^{-1}, the discharge capacity is 490 mAh g^{-1} at the 7th cycle and falls to 275 mAh g^{-1} at the end of the 35th cycle. This clearly indicates drastic capacity fading. On cycling the cell to 1.0 V, however, a capacity in the range 310–340 mAh g^{-1} (at 60 mA g^{-1}) is fairly stable up to 110 cycles as shown in Fig. 5b. This corresponds to 3.3 (±0.2) mol of recyclable Li, as compared with the theoretical value of 4.4 Li.

The higher capacity values observed for $NaFeSnO_4$ on cycling to 3.0 V is understood by the fact that the reactions expressed by Eqs. (4)–(6) contribute to the capacity. The capacity up to 1 V is obtained from the reversible reaction represented by Eq. (4). For Sn-based compounds, it is known that the voltage window of operation is crucial to cycling performance [3,6,20–22] as has been observed for $NaFeSnO_4$. The Na and Fe atoms appear to act as 'spectators' in the voltage range 0.005–1.0 V.

The compounds $NaFeSnO_4$ and $Li_{0.5}Ca_{0.5}(Fe_{1.5}Sn_{0.5})O_4$ display different performance on cycling to an upper cut-off voltage of 3.0 V (Fig. 5). The former shows drastic capacity fading, while the latter has better cycling stability. It should be recalled that in both the compounds, the reversible capacity is contributed by the reaction shown in Eqs. (4)–(6) up to 3.0 V cycling. As mentioned earlier, however, the voltage profiles for the compounds are qualitatively different for the first-charge and subsequent discharge–charge cycles: $NaFeSnO_4$ gives clear two-plateau behaviour and $Li_{0.5}Ca_{0.5}(Fe_{1.5}Sn_{0.5})O_4$ gives an almost continuous profile (Figs. 3 and 4). This may be due to the fact that the Sn:Fe ratio in the former is 1:1 and in the latter it is 1:3. This

makes the Sn in $Li_{0.5}Ca_{0.5}(Fe_{1.5}Sn_{0.5})O_4$ more dispersed in the reduced matrix, whereby a clear identification of the processes corresponding to Eqs. (4)–(6) become difficult. Whereas for $NaFeSnO_4$ the higher Sn content can provide Sn-metal rich regions which makes the processes of Eqs. (4)–(6) clearly distinguishable and hence more efficient oxidation of Sn (Eq. (6)) becomes plausible. The fact that the observed and the calculated (Eqs. (4)–(6a)) capacity values are different for $NaFeSnO_4$ (∼1 Li) but are in close agreement for $Li_{0.5}Ca_{0.5}(Fe_{1.5}Sn_{0.5})O_4$, support the above argument (Table 1). Further, the reversible oxidation of Sn (Eqs. (6a) and (6b) is known to deteriorate the cycling performance in Sn-containing compounds, as seen in the present case. The difference in performance of the above two compounds could also be due to the counter ion present in the matrix. Similar influences of the crystal structure of the starting compounds and the counter ions (spectactor atoms) on the electrochemical performance have been reported for Fe [15] and Sn [3,6] based compounds. The CaO matrix present in $Li_{0.5}Ca_{0.5}(Fe_{1.5}Sn_{0.5})O_4$ may help to give a good cycling performance (0.005–3.0 V) similar to that observed in nano-crystalline $CaSnO_3$ [5,22].

The superior cycling performance observed in $Li_{0.5}Ca_{0.5}(Fe_{1.5}Sn_{0.5})O_4$ on cycling to 3.0 V rather than to 2.5 V, may also be due to reversible formation/decomposition of a polymeric gel-type surface film around the Fe-metal nano-particles, as proposed by Tarascon and co-workers [8,9,14]. Such a film formation can impart stability to the electrode and its reversibility can also contribute to the total capacity. Also, there might exist a threshold electrode potential beyond which the captured metal ionic species will be released, and thereby account for the dissolution of the gel-type layer at higher applied potentials. Thus, at the end of first-discharge, the electrode comprises Fe-metal and $Li_{4.4}Sn$ nano-particles that are embedded in a matrix of Li_2O and CaO, and are surrounded by an inorganic solid electrolyte interphase (SEI) layer with an electrochemically-active polymer film on the outer surface. Such a coating ensures mechanical cohesion between the electrochemically formed nano-grains without hindering the electronic conductivity, and is helpful in maintaining cycleability. The Ca-ions must also be playing a beneficial role since on cycling $NaFeSnO_4$ to a 3.0 V cut-off, a drastic capacity fading is observed (Fig. 5b). In this case, the counter ion matrix (Li and Na) may facilitate the formation of a destructive and resistive surface film which hinders the charge-transfer process and leads to the observed capacity fading.

Cyclic voltammograms (CVs) for $Li_{0.5}Ca_{0.5}(Fe_{1.5}Sn_{0.5})O_4$ and $CaFe_2O_4$ in the voltage window 0.005–3.0 V up to 10 cycles are shown in Fig. 6a and b, respectively. The cv of $NaFeSnO_4$ in the voltage range 0.005–3.0 and 0.005–1.0 V are presented in Fig. 7a and b, respectively. Lithium metal was used for the counter and reference electrodes and the scan rate was 0.058 mV s^{-1}. For all the compounds, the first-discharge profile, commencing from the open-circuit voltage, shows a large decrease in the ΔQ value below

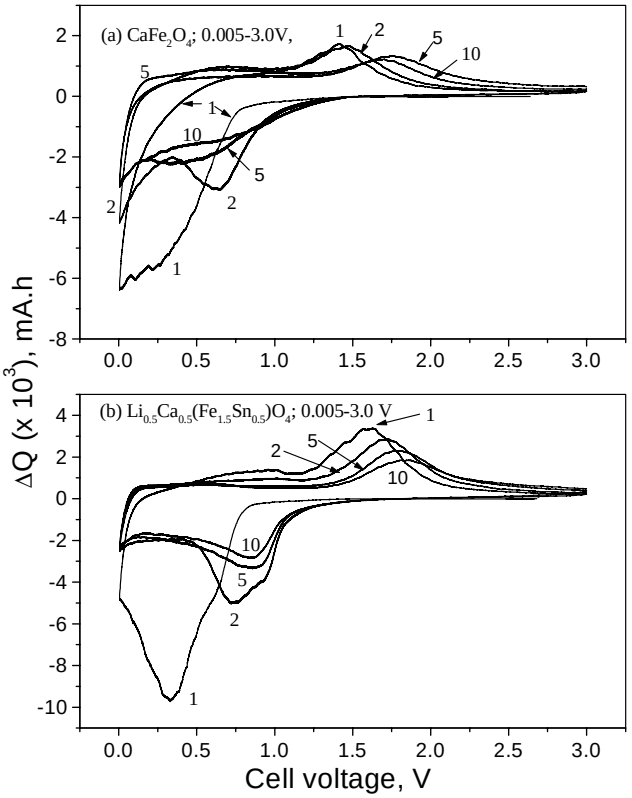

Fig. 6. Cyclic voltammograms (1–10 cycles) for (a) $CaFe_2O_4$ and (b) $Li_{0.5}Ca_{0.5}(Fe_{1.5}Sn_{0.5})O_4$ vs. Li at scan rate of 0.058 mV s^{-1} and voltage window 0.005–3.0 V. Only select cycles are shown. Cycle numbers are indicated.

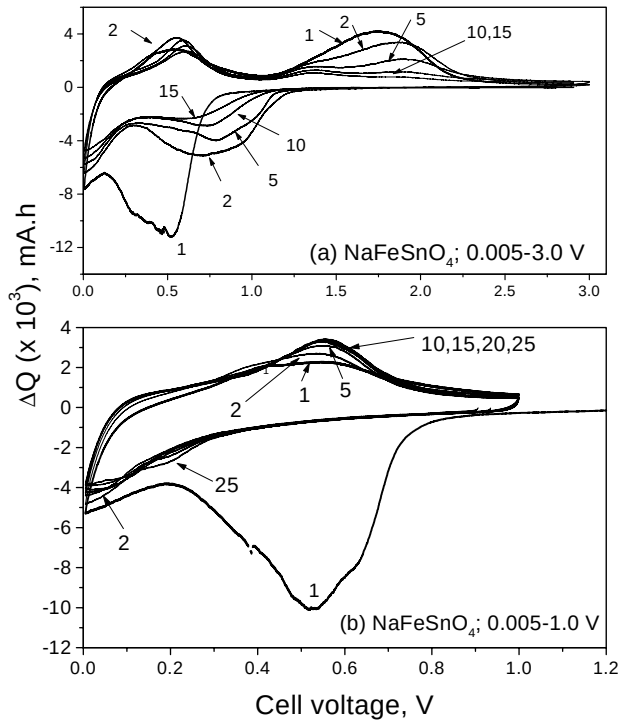

Fig. 7. Cyclic voltammograms for $NaFeSnO_4$ vs. Li at scan rate of 0.058 mV s^{-1}. (a) 1–15 cycles in voltage window 0.005–3.0 V; (b) 1–25 cycles between 0.005 and 1.0 V. Only select cycles are shown. Cycle numbers are indicated.

1.0 V. The profile for $CaFe_2O_4$ does not exhibit any sharp cathodic peaks corresponding to the decomposition reaction, rather the ΔQ value decreases sharply up to the lower cut-off voltage limit of 0.005 V. The second-discharge profile of $CaFe_2O_4$ has a cathodic peak at around 0.63 V that shifts to lower voltages during subsequent cycles with decreased intensity. The first- and second-charge profiles have a well-defined peak at around 1.4 V which gradually shifts to around 1.7 V during 5–10 cycles without much change in the peak area (Fig. 6a). The participation of nano-size Fe-metal particles is obviously reflected in these charge–discharge cycles. The CV profile for the first cycle of $Li_{0.5}Ca_{0.5}(Fe_{1.5}Sn_{0.5})O_4$ displays a well-defined cathodic peak at around 0.3 V with a shoulder at 0.62 V, whereas an anodic peak occurs at around 1.6 V in addition to a broad peak centred at 0.9 V. The cathodic peaks below 1.0 V can be assigned to the formation of Sn and Fe metal particles and alloy ($Li_{4.4}Sn$). The anodic peak at 0.9 V is due to the de-alloying of $Li_{4.4}Sn$, whereas that at 1.6 V is due to the participation of the Fe–FeO couple similar to $CaFe_2O_4$. The second-cycle cathodic peaks occur at 0.75 and 0.9 V, which merge in to one peak followed by a decrease in peak-intensity during 5–10 cycles (Fig. 6b). During these cycles, the anodic peak at 0.9 V is suppressed and the second peak gradually shifts from 1.6 to 1.8 V and decreases in intensity. This probably reflects the increasing cell impedance and indicates capacity-fading in the material on cycling which, in fact, is also seen in galvanostatic cycling (Fig. 5a).

The CV of $NaFeSnO_4$ has been recorded in two voltage ranges to delineate clearly the contributions of Sn and Fe to the charge–discharge processes. When scanned between 0.005 and 3.0 V, the first-cathodic (discharge) peak is broad, i.e. from 0.15 to 0.84 V, and corresponds to the destruction of the crystal structure and the formation of Sn-metal, its alloy ($Li_{4.4}Sn$), and Fe-metal particles. $NaFeSnO_4$ shows two distinct peaks in the anodic scan, one at 0.55 V assigned to de-alloying of $Li_{4.4}Sn$ (reverse reaction of Eq. (4)) and the second at ~1.76 V (Fig. 7a). The latter peak has an intensity which decreases with cycling, and can be assigned to the oxidation of both Fe and Sn (reactions given by Eqs.(5) and (6)) as described earlier. During cycling (2–15 cycles, Fig. 7), the peak at 0.55 V and its intensity remain unaffected whereas that at 1.7 V shifts to higher voltages and its intensity decreases. The CV of $NaFeSnO_4$, up to a cut-off voltage of 1.0 V, where only the reaction of Eq. (4) takes place, shows overlapping anodic peaks from 5 to 25 cycles. This indicates very good cycleability, and thus stability of the compound, as is clearly seen in the capacity data of Fig. 5b. Thus, the CV profiles of the three compounds corroborate the galvanostatic cycling data.

4. Conclusion

Pure and Sn-substituted *iso*-structural ferrites, $CaFe_2O_4$, $Li_{0.5}Ca_{0.5}(Fe_{1.5}Sn_{0.5})O_4$ and $NaFeSnO_4$ have been synthesized, characterized by X-ray diffraction and SEM and, evaluated as cathodes versus Li metal by galvanostatic tests and cyclic voltammetry. $CaFe_2O_4$ gives capacity values which range from 200 to 230 mAh g^{-1} and up to the 15th cycle at 60 mA g^{-1} and in the range 0.005–2.5 V versus Li metal. At the end of 50 cycles, the capacity drops to l60 mAh g^{-1}, which indicates some capacity fading. The achievable capacity values can be enhanced in the compound $Li_{0.5}Ca_{0.5}(Fe_{1.5}Sn_{0.5})O_4$ (450 mAh g^{-1} at 15th cycle falling to 405 mAh g^{-1} at the end of 50 cycles, at 60 mA g^{-1}) but at a higher cut-off voltage (0.005–3.0 V). This higher charging voltage does not show much improvement in charge–discharge capacities but appears to be crucial in reducing capacity fading in $CaFe_2O_4$ and $Li_{0.5}Ca_{0.5}(Fe_{1.5}Sn_{0.5})O_4$. The compound $NaFeSnO_4$ shows drastic capacity fading on cycling to 3.0 V, whereas a very good cycling performance (310–340 mAh g^{-1} stable up to 110 cycles at 60 mA g^{-1}) is obtained between 0.005 and 1.0 V. Pure and Sn-substituted ferrites display qualitative differences in their CV profiles during the first reduction cycle and the profiles on repeated cycling are complimentary to the galvanostatic cycling data.

On comparing the performance of $NaFeSnO_4$ and $Li_{0.5}Ca_{0.5}(Fe_{1.5}Sn_{0.5})O_4$ on cycling in the range 0.005–3.0 V, it is clear that Ca plays a beneficial role in reducing capacity fading. From the observed electrochemical behaviour, the reaction mechanism in these compounds can be explained in terms of structural destruction with the formation of nano-particles of Fe (and Sn and Li–Sn alloy formation in Sn-containing compounds) during the first discharge. The reversible capacities on the subsequent cycles are due to the displacement reaction of these metal particles with Li_2O and Li–Sn de-alloying–alloying reaction. The results for $CaFe_2O_4$ and $Li_{0.5}Ca_{0.5}(Fe_{1.5}Sn_{0.5})O_4$ are in broad agreement with those reported by other workers [17]. The reversible capacities for the present Sn-containing compounds compare very well with that shown by graphite; the average potential range of operation is ~0.5 V for $NaFeSnO_4$ and ~1.5 V for $Li_{0.5}Ca_{0.5}(Fe_{1.5}Sn_{0.5})O_4$. The compounds are therefore promising anode materials for Li-ion batteries.

References

[1] M. Winter, J.O. Besenhard, M.E. Spahr, P. Novak, Adv. Mater. 10 (1998) 725.
[2] Y. Idota, A. Matsufusi, Y. Maekawa, Science 276 (1997) 1395.
[3] I.A. Courtney, J.R. Dahn, J. Electrochem. Soc. 144 (1997) 2943.
[4] M. Mohamedi, S.-J. Lee, D. Takahashi, M. Nishizawa, T. Itoh, I. Uchida, Electrochim. Acta 46 (2001) 1161.
[5] N. Sharma, K.M. Shaju, G.V. Subba Rao, B.V.R. Chowdari, Electrochem. Commun. 4 (2002) 947.
[6] M. Behm, J.T.S. Irvine, Electrochim. Acta 47 (2002) 1727.
[7] M. Winter, J.O. Besenhard, Electrochim. Acta 45 (1999) 31.
[8] P. Poizot, S. Laruelle, S. Grugeon, L. Dupont, J.-M. Tarascon, Nature 407 (2000) 496.
[9] S. Laruelle, S. Grugeon, P. Poizot, M. Dolle, L. Dupont, J.-M. Tarascon, J. Electrochem. Soc. 149 (2002) A627.

[10] M.N. Obrovac, R.A. Dunlap, R.J. Sanderson, J.R. Dahn, J. Electrochem. Soc. 148 (2001) A576.
[11] L.F. Nazar, G. Goward, F. Leroux, M. Duncan, H. Huang, T. Kerr, J. Gaubicher, Int. J. Inorg. Mater. 3 (2001) 191.
[12] G.X. Wang, Y. Chen, K. Konstantinov, M. Lindsay, H.K. Liu, S.X. Dou, J. Power Sources 109 (2002) 142.
[13] G.X. Wang, Y. Chen, K. Konstantinov, J. Yao, J-ho Ahn, H.K. Liu, S.X. Dou, J. Alloys Comp. 340 (2002) L5.
[14] D. Larcher, G. Sudant, J.-B. Leriche, Y. Chabre, J.-M. Tarascon, J. Electrochem. Soc. 149 (2002) A234.
[15] A. Ibarra-Palos, C. Darie, O. Proux, J.L. Hazemann, L. Aldon, J.C. Jumas, M. Morcrette, P. Strobel, Chem. Mater. 14 (2002) 1166.
[16] J.L.C. Rowsell, J. Gaubicher, L.F. Nazar, J. Power Sources 97–98 (2001) 254.
[17] M.J. Duncan, L.F. Nazar, Mater. Res. Soc. Symp. Proc. 548 (1999) 71.
[18] F. Archaimbault, P. Odier, J. Choisnet, Solid State Ionics. 28–30 (1988) 1357.
[19] F. Archaimbault, J. Choisnet, M. Rautureau, Euro. J. Solid St. Inorg. Chem. 25 (1988) 573.
[20] P.A. Connor, J.T.S. Irvine, J. Power Sources 97–98 (2001) 223.
[21] P.A. Connor, J.T.S. Irvine, Electrochim. Acta 47 (2002) 2885.
[22] N. Sharma, K.M. Shaju, G.V. Subba Rao, B.V.R. Chowdari, in: B.V.R. Chowdari, S.R.S. Prabaharan, M. Yahaya, I.A. Talib (Eds.), Solid State Ionics: Trends in The New Millennium, World Scientific, Singapore, 2002, p. 87.